An Integrated Design of Planar Three-dimensional Magnetometers Powered by Novel Flux Guides

Van Su Luong[1,2]*

[1]*Faculty of Electrical and Electronic Engineering, Phenikaa University, Hanoi 12116, Vietnam*
[2]*Phenikaa Research and Technology Institute (PRATI), A&A Green Phoenix Group, 167 Hoang Ngan, Hanoi 11313, Vietnam*

This paper presents a new framework for integrating a planar three-dimensional (3D) magnetometer, featuring high accuracy and reduced size. Sensing elements in this design are magnetoresistance (GMR) sensors, which generally exhibit good in-plane sensitivity but limiting performance when working out-of-plane. Therefore, to improve the out-of-plane sensing ability of the GMR sensors, we design a flux guide (FG) to redirect the out-of-plane magnetic field component to the sensitive plane of the sensors. In doing so, a Ni-Zn cubic FG, combined with a full-bridge of GMR, is exploited for z-sensing axis detection. The cross-detection minimization of in-plane magnetic fields is optimized by an FG rotated by 45° in the x-y axes. Moreover, for boosting the planar sensitivity, two half-bridge GMRs are incorporated into a cross-shaped flux concentrator, working as a full-bridge sensor. The performance of the proposed design is simulated, as well as estimated the sensing features.

Keywords : magnetic sensor, magnetometer, flux guide, GMR, 3D-magnetometers

1. Introduction

Magnetoresistance (MR) sensors have recently attracted much attention due to their high potential in a wide range of applications, including biomedical devices, flexible electronics, contactless switches, navigations, and smart transportations [1-3]. Notably, in the new era of the 4.0 industry [4], electronic devices tend to be upgraded towards multifunctional and efficient devices, also called smart devices, which are highly demanded in smart things, including homes, healthcare systems, or transportations [5]. The critical factor toward a world of smart devices is the possibility of collecting a tremendous amount of information by using sensors. Therefore, sensors with advanced features, e.g., multidimensional detection, low-cost, low-power consumption, miniature size, and compatible with integrated circuit (IC) technology, will be the chosen candidates.

In fulfilling the above requirements, the magnetic sensor needs to be developed with criteria, including multiple sensing axes, high sensitivity, and high resolution, while using the planar fabrication fully compatible with recent

IC technology [6]. In the three-dimensional (3D) magnetometer structure, three sensors are traditionally used by aligned orthogonally to each other along three coordinates x, y, and z. Such designs lead to a critical limitation in miniaturizing and integrating the MR system into portable devices. So far, many designs of the 3D-magnetoresistive sensor using planar technology have been realized, e.g., anisotropy magnetoresistance (AMR) sensor on a V-groove substrate [7], giant magnetoresistance (GMR) with a slope flux guide (FG) [8], S-shaped FG for unidirectional GMR [9], or cubic FG [10]. Despite such designs have different benefits, several critical points that need to be improved and redesigned;

For instance, in the V-groove AMR design [7] or slope FG for GMR [11]: (1) the out-of-plane sensitivity is limited by the angle of the crystalline silicon (Si) wafers and the wafer thickness; (2) the anisotropic etching to form V-groove uses a unique type of (100) silicon wafer; (3) the uniformity of thin films that are fabricated on the slope depends strongly on the slope roughness and deposition technique. Jue Chen *et al.* [9] have simulated the design of an S-shaped FG, which allows us to solve a complicated process in defining the pinned sensing direction of the GMR. However, the S-shaped FG usually requires a large space facing spatial resolution and significant angle error. Besides, the fabrication of the S-

*Corresponding author: Tel: +84-986-235-122
Fax: +84-242-2180-336, e-mail: su.luongvan@phenikaa-uni.edu.vn

shaped FG for the vertical detection is practically complicated.

In our previous work [10], we proposed a design of a 3D-magnetometer that used a cubic FG and a single GMR bridge. One prominent point is that a single full-bridge is formed to detect three magnetic field components. However, the time switching between each sensing axis appeared as a drawback, limiting the real-time response of the sensor.

In tackling the above challenges, we propose in this report a new design of 3D-magnetometer using the planar technique, flux-concentrator for in-plane GMR sensor, and a cubic FG for z-component detection. In such an approach, the step of anisotropic etching of silicon wafer is no longer necessary. The sensing circuits x, y, and z are separated, where x and y sensing axes are formed using two half-bridge working as a full-bridge for enhancing the sensitivity, and z-axis using a single full-bridge to cancel out the cross-detection by the x and y field components. The features of the design are simulated using the finite element method and analyzed in the following sections.

2. Sensor Design

2.1. Flux guide principle

The concept of the 3D-magnetometer is illustrated in Fig. 1. In the x-y plane, the flux concentrators (FC) are made from Mu-metal (NiFeCuMo) with an ultra-high permeability (~100,000). In our previous work [12], the relative permeability of sputtered Mu-metal thin film could reach up to ~8000. When the FC is placed in x-y magnetic field components, the flux is concentrated by the Mu-metal films. Consequently, the flux density in the FC's gap is significantly amplified, which promotes a high sensitivity of the GMR sensors. An intrinsic feature of GMR sensors is in-plane sensitivity, and there are two typical structures of GMR sensors, including a multilayer structure (superlattice) with the antiferromagnetic coupling effect and a pinning spin valve (PSV). The response of the GMR multilayer is V-shaped and unipolar output. Whereas, the output of the PSV type is bipolar response and is very sensitive to the zero-field region. However, the PSV type is more complicated to fabricate than the multilayer type because of the complicated fabrication processes (e.g., either post field annealing or bias field during deposition). Additionally, PSV requires high-cost materials, such as FeMn, IrMn, Ru. In this work, therefore, we aim to use the multilayer GMR structure for sensing elements and propose an innovative technique that provides the bipolar response from unipolar GMR and simultaneously enhance the sensitivity for multilayer GMR.

For sensing the vertical magnetic field component (z-axis), a cubic FG is made of Ni-Zn with a high permeability of ~2000. When the z-axis magnetic field component is applied along the vertical direction of the FG, the flux will be bent to the x-y plane, and GMR can detect easily. To replace the method that uses the decoupling
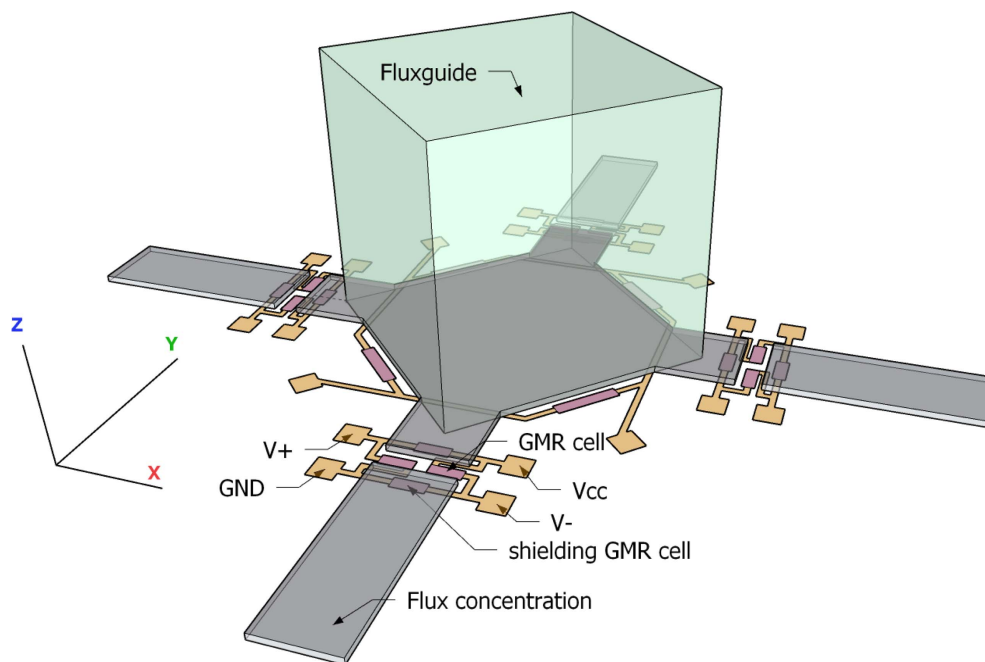

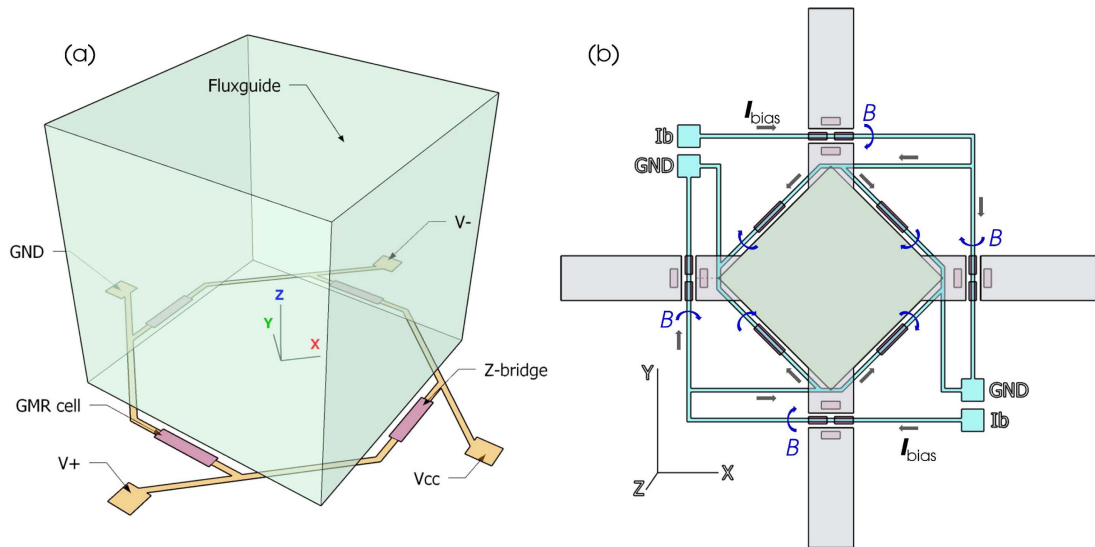**Fig. 1.** (Color online) The design concept of the 3D-magnetometer.

Fig. 2. (Color online) (a) The design of the flux guide for *z*-sensing axes, and (b) the current line is to bias the operation points of the GMR sensors.

magnetic field component by combining of *x* and *y* sensors for the *z*-axis detection, we use a full-bridge separately for the *z*-axis. The GMR element of the *z*-bridge is located near the outer edge at the bottom of the cubic FG. A current line is proposed to bias the response of the multilayer GMR elements from unipolar into bipolar outputs, as shown in Fig. 2(b). The magnetic field strength induced by a current line can be estimated via the following equation:

$$B = \mu_0 I / 2\pi r \qquad (1)$$

where B is the magnetic field, I is the biased current, and r is the distance to the current line, and $\mu_0 = 4\pi \times 10^{-7}$ T.m/A is the permeability of free space.

2.2. Simulation of the proposed design

Cubic FG is designed in the dimension of $1000 \times 1000 \times 1000$ μm³; thus, its aspect ratio is one, as shown in Fig. 2(a). It has been proved that the apparent permeability of the FG is dependent on the given aspect ratio and the initial permeability of the Ni-Zn material [13]. A magnetic field of 50 μT is applied vertically to predict the sufficient flux at the GMR positions and to estimate the *z*-axis sensitivity.

Since the measurement of the flux gain in the gap of the FC is an experimental challenge. The finite element method is considered to validate the design and estimate the flux gain factor in the gap of the FC and the flux bending factor of the FG. Based on our previous works on the FC [12], the simulation is set up under the technical parameters consisting of a length of $L = 1500$ μm, a width

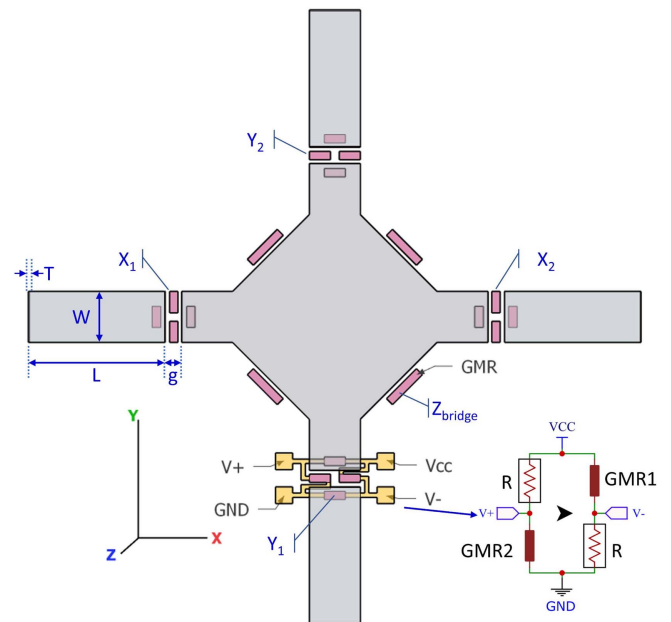**Fig. 3.** (Color online) The design of the flux concentrator for *x-y* sensing axes.

of $W = 300$ μm, aspect ratio $W/L = 0.2$, $\mu_r = 8000$, T varied from 1 μm to 6 μm, the gap width from 10 μm to 50 μm, under a static magnetic field of 50 μT, as illustrated in Fig. 3. The gain factor can be estimated using the following equation:

$$Gain = B_{gap} / B_{ext} \qquad (2)$$

The simulated materials, including Ni-Zn, Mu-metal, and vacuum, are used in the available library of the

simulator. The boundary box is set in a dimension of 10 mm × 10 mm, and the mesh is set automatically.

The magnetic vector potential can be defined as follows:

$$\vec{B} = \nabla \times \vec{A} \qquad (3)$$

The polar vector field $\vec{A}$ is proportional to the current. So, the positive ($+A_0$) and negative ($-A_0$) vector potentials can be defined by the current direction. Suppose, we set the intensity of the vector potential $\vec{A}$ at the boundary of $x = -x_0$ and $x = +x_0$ to $-A_0$ and $+A_0$, respectively. The following equations can estimate the relationship between the magnetic field and vector potential A_0:

$$\vec{B} = B_0 \hat{a}_y = \frac{A_0}{x_0} \hat{a}_y \qquad (4)$$

$$A_0 = B_0 x_0 \qquad (5)$$

So, for example, at $x_0 = 10$ mm, and the applied magnetic field is $B_0 = 50 \mu T$, thus, the boundary of the vector potential is $A_0 = 0.5 \times 10^{-6} wb/m$. The $\pm A_0$ values are used to set the boundary of the 50 μT applied field in the simulator. The flux concentrator is located at the position $x = 0$.

3. Results and Discussion

3.1. In-plane detection

The intrinsic feature of the GMR is the in-plane sensitive response. The FC is used to boost the sensitivity and suppress the cross detection between the x and y sensing axis. The distribution of the flux density for the x-sensing axis exposing in the B_x is illustrated in Fig. 4. Flux density is concentrated and uniform in the x-axis

gaps. Whereas, in the other gaps (y-axis), the flux density is attenuated. The high concentrated flux is denoted by the high density of the flux lines in Fig. 4(a) or the green color in Fig. 4(b). In contrast, the flux attenuation is denoted by the few flux line in the gap (Fig. 4a) or dark blue color (Fig. 4b). The influences of the gap size on the flux gain factor under different thicknesses of the FC is estimated, as shown in Fig. 5. The simulation results show that with a larger gap size (g), the gain factor is lower. Besides, the higher thickness of the FC enhances the gain factor. However, in the practical implementation, a thick FC fabricated via physical vapor deposition (sputtering deposition) is not feasible, and thicker FC will raise the hysteresis problem [12]. So, in mitigating such a
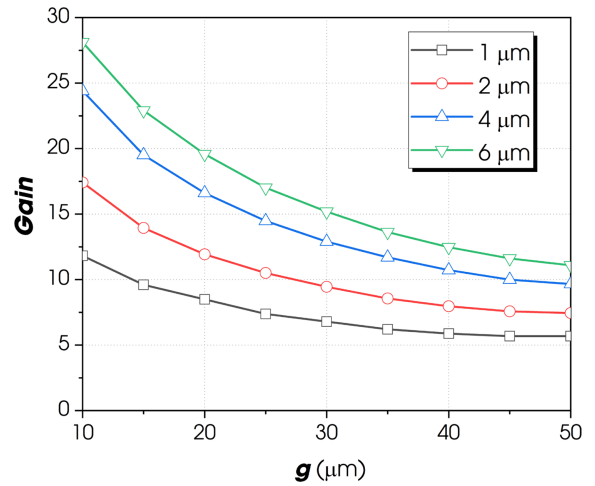

Fig. 5. (Color online) The gain factor of the flux densities under various gap size and thickness (1-6 µm) of the concentrator.
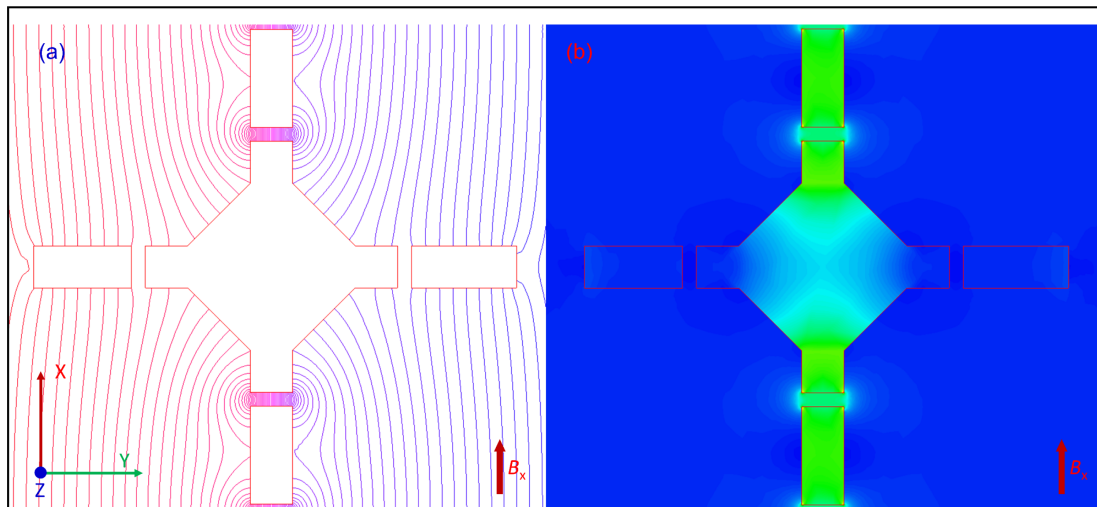

Fig. 4. (Color online) The distribution of the flux density of the designed FC for x-y sensing axes; (a) shown in flux lines distribution, and (b) shown in Bmag.
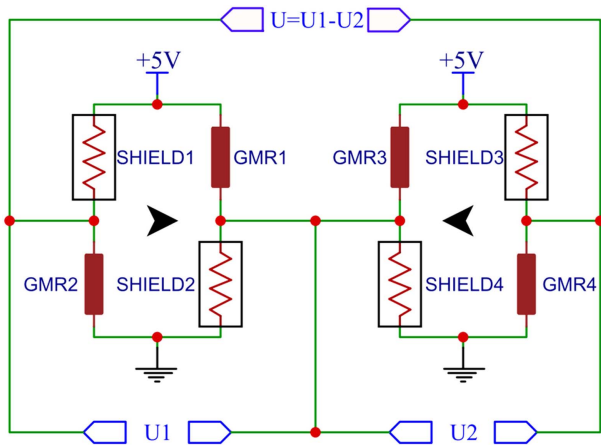
Fig. 6. (Color online) The combined circuit of two half-bridge GMR sensors.
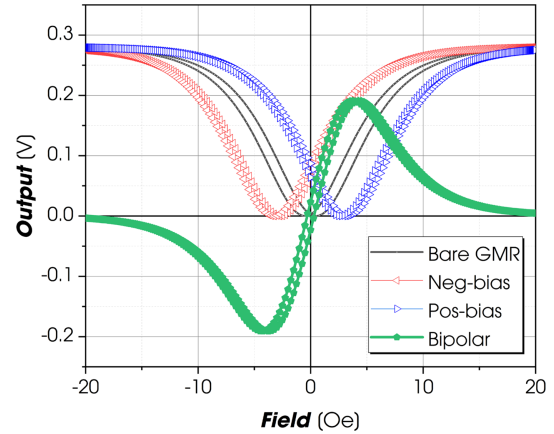

Fig. 7. (Color online) The responses of the GMR sensor, including a bare GMR output, GMR sensors with a negative and positive bias, and the combined GMR sensor with a bipolar response.

problem, a thickness of less than 1 μm is considered. The gain factor can also be improved by narrowing the gap as small as the width of the GMR element.

In the x- and y-axis, two gaps of the FC are incorporated with two half-bridges of GMR sensors. Since the output of the GMR multilayer is a V-shaped curve that is a unipolar response, thus, it cannot be used directly for vector measurements. Interestingly, the V-shaped response of the GMR multilayer can be biased to the linear response sides [14]. Figure 6 shows the schematic of the combined sensor using two half-bridge GMR. The working principle of the circuit can be briefly interpreted as follows;

Suppose that $SHIELD1 = SHIELD2 = R$, and $GMR1 = GMR2 = R+\Delta R$. Hence the output of a half-bridge is expressed as follows:

$$U_1 = V_{cc} \cdot \left[\frac{\Delta R / R}{(2+\Delta R/R)} \right] \qquad (6),$$

Similarly, the U_2 is with a minus sign due to the opposite bias of two half-bridges.

$$U_2 = -V_{cc} \cdot \left[\frac{\Delta R / R}{(2+\Delta R/R)} \right] \qquad (7)$$

Hence, the output of the combined sensor is given by:

$$U = U_1 - U_2 = 2V_{cc} \cdot \left[\frac{\Delta R / R}{(2+\Delta R/R)} \right] \qquad (8)$$

According to the Eq. (8), the output of the combined sensor is double, so that its sensitivity can be duplicated. Besides, the bipolar response of the combined sensor is established, and the V-B curve action like a full-bridge configuration. Figure 7 shows the responses of the GMR multilayer, i.e., the V-B curves consisting of the bare

GMR sensor without magnetic bias, the GMR sensor with a negative and positive bias, and a bipolar response of the combined sensor for the in-plane sensing axes. When the bias magnetic field is zero, two bare GMR sensors are balanced, and they have V-B response in V-shaped curves resulting in their different output is zero, as shown by the open black square curve in Fig. 7. In contrast, when the bias magnetic field is applied, the responses of two GMR sensors are oppositely biased, leading to their different output is unbalanced, and the V-B response of the different output is a bipolar curve, as illustrated by the close green pentagon curve in Fig. 7. It means that the
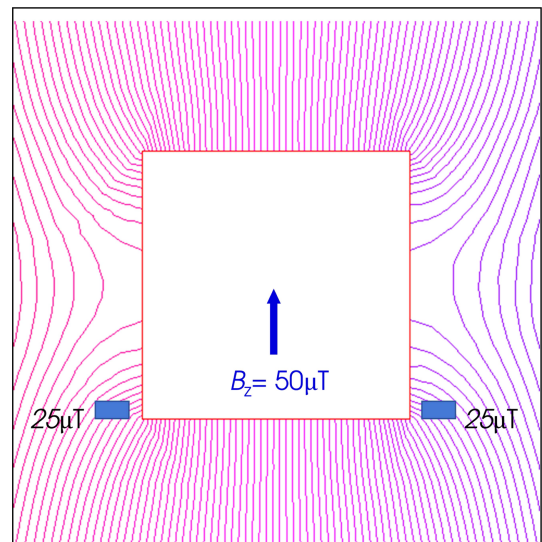

Fig. 8. (Color online) The distribution of the flux density of the cubic flux guide under a uniform static magnetic field of 50 μT, and the field strength of 25 μT at GMR positions (near the outer edge of the FG).

proposed circuit can develop a highly sensitive and bipolar sensor.

3.2. Out-of-plane detection

A flux guide is introduced to redirect the magnetic flux from out-of-plane to in-plane components, which can easily detect co-planar GMRs. Figure 8 shows the bending effect of the flux line induced by the cubic FG. The effective redirection at the GMR cell location is also estimated using the simulation. In practice, the efficient redirection of the FG is impossible to reach 100 %. In the simulation, the boundary condition of 50 μT applied magnetic field generates an attenuated field of 25 μT at the GMR locations; thus, the redirection factor is estimated at 0.5. In other words, the flux gain is about 0.5.

In the z-sensing axis, four GMR elements are biased, as shown in Fig. 9. Besides, the GMR elements are connected to form a full bridge that provides additional advantages as the following interpretations. Suppose that four GMR elements are equal to R because they are fabricated in the same conditions, and ΔR is the MR change of the GMR under an applied magnetic field B. Then the output of the z-axis is given by:

$$V_{out}(B) = V_{cc}.\Delta R/R \qquad (9)$$

Firstly, with $B = B_x$ leads to $GMR1 = GMR3 = R + \Delta R$, and $GMR2 = GMR4 = R - \Delta R$. Consequently, $V+ = V- = (R + \Delta R).V_{cc}/2$ at all value of the B_x, making the output $V_{out}(B_x) = 0$. It means that the z-bridge is insensitive to the x-axis magnetic field component.

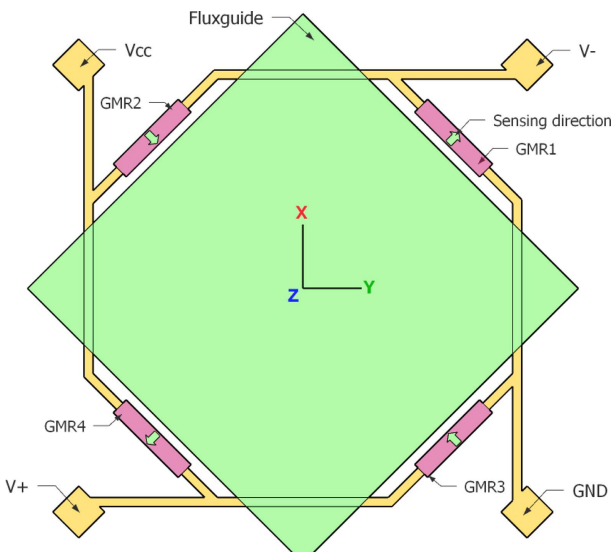Secondly, that is similar to $B = B_y$ makes $GMR1 = GMR2 = R - \Delta R$, and $GMR3 = GMR4 = R + \Delta R$, conse-
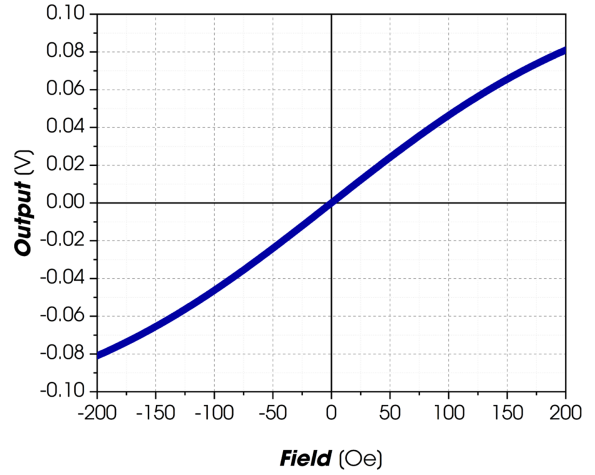
Fig. 10. (Color online) The *V-B* response of the *z*-axis sensor under a gain of 0.5 and an *MR* ratio of 5 %.

quently, $V+ = V- = V_{cc}/2$ with any of B_y, thus, the output of the bridge $V_{out}(B_y) = 0$. It means that the z-axis circuit cancels out the B_y component.

Finally, with $B = B_z$, we have $GMR1 = R - \Delta R$, $GMR2 = R + \Delta R$, $GMR3 = R + \Delta R$, and $GMR4 = R - \Delta R$. Hence, $V+ = (R + \Delta R).V_{cc}/2R$, and $V- = (R - \Delta R).V_{cc}/2R$ result to the output $V_{out}(B_z) = (\Delta R/R).V_{cc}$ indicating that the circuit configuration of the z-bridge is selectively sensitive to the B_z while canceling out the x and y magnetic field components [10].

Based on the hyperbolic tangent model of a GMR full-bridge sensor in our previous report [6]. The sensitivity of the z-bridge (*V/V/Oe*) can be expressed via the following equation;

$$s_B = gain.\frac{MR\%}{(2 + MR\%).B_S} \qquad (10)$$

where *gain* is the flux amplification, s_B is the sensitivity, $MR\%$ is the MR ratio, and B_S is the saturation field.

For example, with a gain factor of 0.5, a 5 % MR can provide a z-axis sensitivity of approximately 0.1 mV/V/Oe. Figure 10 shows the *V-B* response of the z-axis bridge sensor using the proposed FG with a linear range of $\pm$ 50 Oe.

4. Conclusion

We have proposed a new integrated 3D magnetometer using GMR sensors and FG technology. The x- and y-sensing axes are designed using two half-bridge of GMR sensors working as a full bridge and a planar flux concentrator for boosting the device sensitivity. The z-sensing axis is developed by a cubic FG to redirect the flux lines from the vertical direction to the in-plane sensitivity of

Fig. 9. (Color online) Top view of the z-bridge configuration with the designed flux guide.

the GMR sensors. The bias point of GMR is well controlled by a current line generating the bias magnetic fields. The notable advantage of the z-axis detection is that the bridge is selectively sensitive to the z- magnetic field component while canceling out the x and y-magnetic fields. Our future work focuses on how to precisely cut the cubic flux guide and building up an alignment system to locate flux guides accurately.

Acknowledgments

References

[1] C. Zheng, K. Zhu, S. C. D. Freitas, J. Chang, J. E. Davies, P. Eames, P. P. Freitas, O. Kazakova, C. Kim, C. Leung, S. Liou, A. Ognev, S. N. Piramanayagam, P. Ripka, A. Samardak, K. Shin, S. Tong, M. Tung, S. X. Wang, S. Xue, X. Yin, and P. W. T. Pong, IEEE Trans. Magn. **55**, 1 (2019).

[2] A. Grosz, M. J. Haji-Sheikh, and S. C. Mukhopadhyay, High sensitivity magnetometers, Springer International Publishing, Switzerland 225 (2017).

[3] P. P. Freitas, F. A. Cardoso, V. C. Martins, S. A. M. Martins, J. Loureiro, J. Amaral, R. C. Chaves, S. Cardoso, L. P. Fonseca, A. M. Sebastião, M. Pannetier-Lecoeur, and C. Fermon, Lab on a Chip. **12**, 5467 (2012).

[4] A. Schütze, N. Helwig, and T. Schneider, J. Sens. Sens. Syst. **7**, 359 (2018).

[5] X. Liu, K. H. Lam, K. Zhu, C. Zheng, X. Li, Y. Du, C. Liu, and P. W. T. Pong, IEEE Trans. Magn. **55**, 1 (2019).

[6] V. S. Luong, Y. H. Su, C. C. Lu, J. T. Jeng, J. H. Hsu, M. H. Liao, J. C. Wu, M. H. Lai, and C. R. Chang, IEEE Trans. Nanotechnol. **17**, 11 (2018).

[7] F. C. S. da Silva, S. T. Halloran, L. Yuan, and D. P. Pappas, Appl. Phys. Lett. **92**, 142502 (2008).

[8] J. Zhao, W. Tian, Q. Zhang, M. Pan, J. Hu, D. Chen, and F. Luo, IEEE Trans. Magn. **49**, 5301 (2013).

[9] J. Chen, M. C. Wurz, A. Belski, and L. Rissing, IEEE Trans. Magn. **48**, 1481 (2012).

[10] V. S. Luong, J. T. Jeng, B. L. Lai, J. H. Hsu, C. R. Chang, and C. C. Lu, IEEE Trans. Magn. **51**, 1 (2015).

[11] J. Zhao, J. Hu, W. Tian, J. Hu, and M. Pan, IEEE Trans. Magn. **51**, 1 (2015).

[12] V. S. Luong, A. T. Nguyen, T. L. Nguyen, A. T. Nguyen, and Q. K. Hoang, IEEE Trans. Magn. **54**, 1 (2018).

[13] D. X. Chen, J. A. Brug, and R. B. Goldfarb, IEEE Trans. Magn. **27**, 3601 (1991).

[14] C. H. Smith and R. W. Schneider, Sensors EXPO1999, Baltimore May 1 (1999).